Numerical Simulation Study on the Water Blocking Effect of Circular Inclined Piers

Xiaoquan Yang*

School of Civil Engineering, Lanzhou Jiaotong University, Lanzhou, Gansu, 730070, China

*Email: 465873768@qq.com

Abstract. In contemporary bridge construction, stringent requirements are placed on the water-blocking effect of bridge piers; however, the precision of current analysis methods is relatively low. To better analyze the water-blocking effect of circular skewed bridge piers, numerical simulation methods were employed to derive a global water-blocking effect coefficient and to analyze the influence of various factors on the magnitude of backwater around pier groups. Simulation results indicate that the water-blocking effect of bridge piers is directly proportional to flow velocity, water depth, discharge, and the skew angle between the pier and the river channel. Moreover, the study derived a global water-blocking effect formula and verified its applicability. This research not only enhances the precision of pier design but also provides important theoretical support for bridge engineering, contributing significantly to industry development.

Keywords: skew angle; bridge pier; froude number; water-blocking effect coefficient; numerical simulation

1 Introduction

In bridge engineering, the water-blocking effect of piers is a critical design factor. With the continuous advancement of transportation infrastructure and the increase in the number and scale of bridges, studying the water-blocking effect of piers has become even more significant [1-2].Currently, research on the water-blocking effect of bridge piers mainly focuses on experimental observations and empirical formulas. However, there is still room for improvement in terms of accuracy and general applicability [3].The current state of research on the water-blocking effect of piers shows that while some empirical formulas and models exist for prediction and evaluation, most proposed methods are limited to specific working conditions and pier shapes, making them difficult to apply broadly [4].

Deng Shaoyun et al. [5] proposed a formula for calculating water flow resistance based on resistance coefficients, providing theoretical support for the derivation of the global water-blocking effect coefficient and formula in this paper. Zhang Tingrong et al. [6] proposed a formula for calculating the water-blocking rate (water-blocking ratio) from an energy perspective and validated this formula through numerical flume ex-

Y. Zhang et al. (eds.), *Proceedings of the 2024 10th International Conference on Architectural, Civil and Hydraulic Engineering (ICACHE 2024)*, Advances in Engineering Research 259,
https://doi.org/10.2991/978-94-6463-658-1_32

periments, offering a new perspective on understanding the impact of piers on water flow energy loss. Wei Shuai et al. [7] used a two-dimensional hydrodynamic model to study the effect of pier arrangement on backwater height, revealing the mechanism by which pier alignment influences upstream water levels. Gao Pengcheng et al. [8] explored the protective effect of anti-scour plates for round-ended piers using Fluent software and analyzed the scouring and flow characteristics around the piers. Moreover, existing studies mostly focus on analyzing individual influencing factors and lack in-depth research on the combined effects of multiple factors [9].

To address the limitations of previous studies, this research proposes a numerical simulation method to comprehensively analyze the water-blocking effect of circular inclined piers. Building on and extending the research ideas of Deng Shaoyun [5] and Zhang Tingrong [6], which were based on resistance coefficients and energy analysis, this study develops an accurate hydraulic model and conducts numerical simulations to derive a global water-blocking effect coefficient and formula. This method can quantify the overall impact of piers on water flow, extending the applicability of previous methods. Compared to earlier research, this approach not only applies to a wider range of working conditions and pier shapes but also considers various influencing factors, such as pier shape, skew angle, arrangement, and flow conditions, providing an in-depth analysis of their combined effects. The innovation of this study lies in the introduction of the global water-blocking effect coefficient and formula, making the evaluation of pier water-blocking effects more comprehensive and precise. This not only provides a more universal theoretical basis for bridge design but also helps engineers more effectively predict and mitigate the adverse effects of piers on water flow, thereby optimizing bridge engineering design.

2 Numerical Simulation

2.1 Numerical Simulation Models and Methods

Compared to the standard k-ε model, the RNG k-ε model has been optimized in two key aspects. First, it improves the calculation method of turbulent dynamic viscosity, particularly by considering the rotational effects in mean flows and rotating flows. This enhances the model's predictive capability under transient flows and the influence of streamline curvature. Second, a new term is introduced into the ε equation to more accurately reflect the time-averaged rate of change of the main flow, making the generation term in the RNG k-ε model not only related to flow characteristics but also further improving the precision of the ε equation. For these reasons, the RNG k-ε turbulence model was chosen for the simulation calculations in this paper.

To better simulate the water-blocking effect and flow field around circular inclined piers, numerical simulation models and methods are required [10].The VOF model in Fluent software offers accurate control of liquid levels and simplifies the setting of initial and boundary conditions, making it suitable for simulating the flow in this experiment [11-12].Therefore, this study utilizes Fluent software for simulating the water-blocking effect and flow field around circular inclined piers, using the VOF method to track the free surface. Additionally, the numerical simulation of the turbulence model employs the Reynolds-Averaged Navies-Stokes (RANS) model, which is refined using the RNG k-ε two-equation model [13-14]. The near-wall region is treated using the standard wall function, and the governing equations are discretized using a first-order upwind scheme. The governing equations consist of the continuity equation and the momentum conservation equation. The expression for the continuity equation is shown in Equation (1) [15-16].

$$\frac{\partial_q}{\partial t} + \Delta \cdot (q\vec{u}) = 0 \tag{1}$$

In Equation (1), q represents the fluid density. momentum equation employs the Reynolds-averaged model, and its expression is shown in Equation (2) [17].

$$\frac{\partial u_i}{\partial_t} + \frac{\partial u_i u_j}{\partial x_j} = -\frac{1}{q}\frac{\partial c}{\partial x_i} + \frac{1}{q}\frac{\partial}{\partial x_j}[u(\frac{\partial u_i}{\partial x_j} + \frac{\partial u_j}{\partial x_i} - \frac{2}{3}\delta_{ij}\frac{\partial u_k}{\partial x_k}] + \frac{\partial}{\partial x_j}(-\overline{u_i u_j}) + f_i \tag{2}$$

In Equation (2), (i, j, k) represent the three-dimensional flow directions, t denotes time, and f_i represents the body force. The two equations of the RNG k-ε model are shown in Equation (3).

$$\begin{cases} \frac{\partial}{\partial_t}(qk) + \frac{\partial}{\partial x_i}(qku_i) = \frac{\partial}{\partial x_j}(a_k u_{eff}\frac{\partial k}{\partial x_j}) + G_k + q\varepsilon \\ \frac{\partial}{\partial_t}(q\varepsilon) + \frac{\partial}{\partial x_i}(q\varepsilon u_i) = \frac{\partial}{\partial x_j}(a_k u_{eff}\frac{\partial \varepsilon}{\partial x_j}) + \frac{C_{1\varepsilon}^*}{k}G_k + C_{2\varepsilon}q\frac{\varepsilon^2}{k} \end{cases} \tag{3}$$

In Equation (3), ε represents the turbulent kinetic energy, and k denotes the turbulent dissipation rate. The expression for the wall function is shown in Equation (4).

$$\begin{cases} u^+ = \frac{u}{u_t} = \frac{u}{\sqrt{\tau / q}} \\ y^+ = \Delta\frac{yqu_\tau}{v}\sqrt{\tau / q} \end{cases} \tag{4}$$

In Equation (4), u^+ and y^+ are dimensionless parameters. The expressions for determining the interface position within an infinitesimal element in the VOF model and the density equation in the VOF model are shown in Equation (5).

$$\begin{cases} \frac{F_{water}^{n+1} q_{water}^{n+1} - F_{water}^{n} q_{water}^{n}}{\Delta t} + \sum_f F_{water,f}^{n+1} q_{water}^{n+1} U_f^{n+1} = 0 \\ q = F_{water} q_{water} + F_{air} q_{air} \end{cases} \tag{5}$$

In Equation (5), F_{water} represents the volume fraction of the liquid, F_{air} represents the volume fraction of the gas, and $F_{water} + F_{air} = 1$ .To ensure the smooth operation of the numerical simulation, it is necessary to arrange the computational domain and mesh reasonably and to determine the initial boundary conditions [18]. Due to the high precision and operational simplicity of the nine-square grid method, this study employs this mesh for calculations. The layout of the computational domain and mesh distribution is shown in Figure 1. In Figure 1(a), the computational domain shows a pier with a diameter of 14.25 cm, with the pier set as the origin. After dimensionless normalization of the lengths in the T and Q directions, the lengths in the forward, left, and right directions from the pier are 10D, and the length behind the pier is 5D. The computational domain, the mesh near the pier, and the mesh at the gas-liquid interface are shown in Figures 3(b), (c), and (d), respectively.

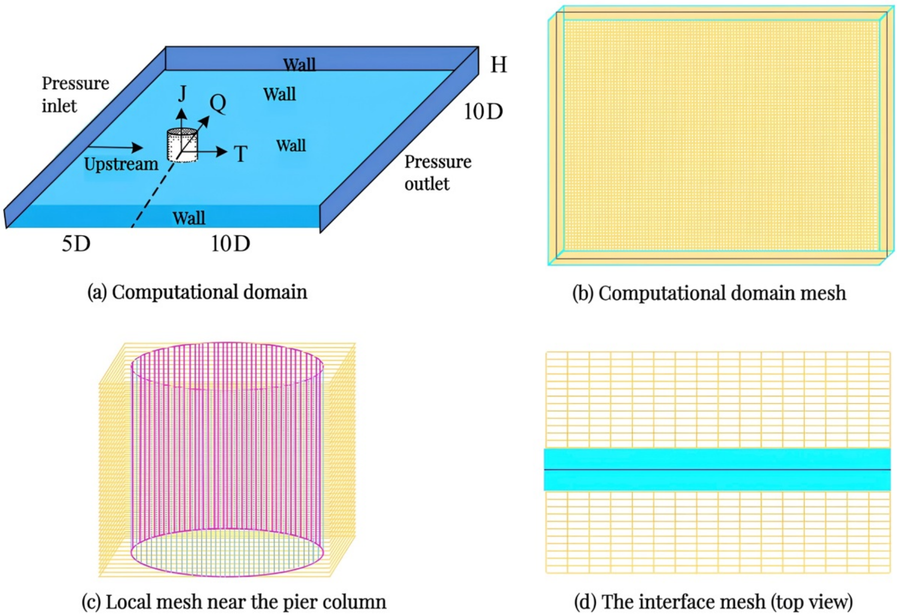

Fig. 1. Computational domain and mesh distribution views

2.2 Construction and Application of Numerical Models

Numerical hydraulic models are scaled three-dimensional physical models of ports and waterways, widely used in the research, design, and evaluation of hydraulic structures to better understand and solve issues related to water resources [19]. Study to better observe and record the changes in the water surface profile before and after the placement of the pier, a numerical hydraulic model of the pier was first constructed. The schematic layout of the hydraulic model is shown in Figure 2.

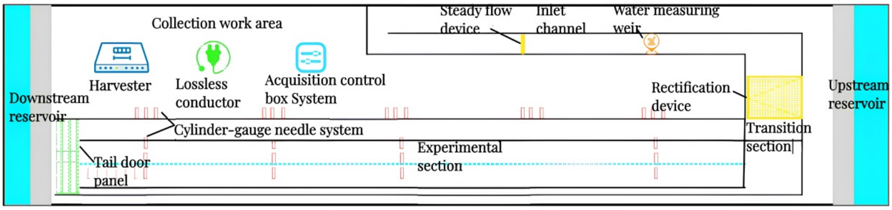

Fig. 2. Schematic diagram of the bridge pier hydraulic model

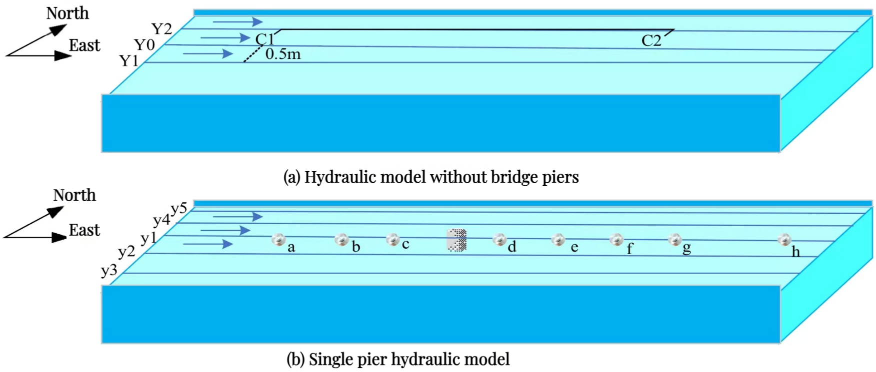

Fig. 3. Layout diagram of the numerical model for the water-blocking effect

As shown in Figure 2, the hydraulic model mainly includes the inlet channel, test section, transition section, data acquisition workspace, and operating condition settings. The test section has a trapezoidal cross-section with a bottom width of 2 m, a top width of 3 m, and a side slope ratio of 3:1. To monitor water level changes in real time, three cylinder-probe devices are installed every 5 m at intervals of 50 cm to monitor cross-sections. A measuring weir and a flow-stabilizing device are installed at the inlet channel to smoothly regulate the flow rate and velocity at the inlet. The transition section is the core part of the hydraulic model; a rectification device is installed in this section to connect the flow between the test section and the inlet channel and adjust the flow into the motion patterns required for the experiment. Eight ultrasonic cameras are placed in the data acquisition workspace, and automatic water level measuring equipment such as non-destructive wires and acquisition control boxes are set up in the dry area. The function of this area is to detect and record changes in the water surface profile. After setting up the hydraulic model as described above, the study discusses the distribution pattern of the water-blocking effect of a characteristic single pier by conducting experiments with and without piers. The experiments are divided into no-pier and single-pier water-blocking effects, and both require the construction of corresponding hydraulic models. In the no-pier hydraulic model, the hydraulic characteristics such as the blockage ratio, energy coefficient, characteristic flow depth, and Reynolds number are 6.1%, 0.017, 0.18, and 1.73×10^4, respectively; in the single-pier hydraulic model, the hydraulic characteristics such as the blockage ratio, energy coefficient, characteristic flow depth, and Reynolds number are 6.1%, 0.005, 0.08, and 1.47×10⁴, respectively. The specific experimental arrangements of the two hydraulic models are shown in Figure 3.

In Figure 3(a), C1 and C2 represent two cross-sections spaced 6.8 meters apart along the flow direction, while Y0, Y1, and Y2 denote three measurement axes in the northern direction, each spaced 0.5 meters apart. As shown in Figure 3(b), the single-pier experiment adds an upright circular pier as the pier model based on the no-pier experimental setup. Taking the pier as the origin, eight ultrasonic probes are arranged at positions a, b, c, d, e, f, g, and h along the east axis. The probes at positions a, b, and c are used to collect water levels in front of the pier, while those at positions d, e, f, g, and h collect water levels behind the pier. Additionally, the study sets up five measurement axes in the northern direction and applies dimensionless processing to the measurement position coordinates.

3 Analysis of Numerical Simulation Results

3.1 Derivation of the Global Water-Blocking Effect Coefficient of Bridge Piers

In this study, based on data from numerical simulations, the global water-blocking effect coefficient is derived from both the force analysis perspective and the energy conservation perspective. From the force perspective, the formula derivation assumes that Section 1 represents the upstream initial cross-section, and Section 3 represents the downstream cross-section where the water level returns to normal. By combining the mathematical expression of a cylinder with characteristic length D and Newton's Third Law, we obtain the momentum equation for a single water body around the pier, which is then rewritten and derived to obtain Equation (6).

$$\begin{cases} F_p - F_D = \rho Q V \\ F_D = \dfrac{1}{2} C_D \rho V^2 A_{pier} \\ F_p = F_{p\_1} - F_{p\_3} = \int_0^{h_1} \rho g y B dy - \int_0^{h_3} \rho g y B dy \end{cases} \tag{6}$$

In Equation (6), A_{pier} represents the water-blocking area of the bridge pier, C_D denotes the drag coefficient of flow around a cylinder, D is the characteristic length, F_p - F_D indicates the pressure difference before and after the bridge pier, V represents the average flow velocity at the cross-section, and Q is the upstream inflow rate. By deriving Equation (6) and establishing the cross-sectional continuity equation, we simplify it to obtain the average cross-sectional drag coefficient, with its calculation expression shown in Equation (7).

$$\begin{cases} C_D = 2[\frac{3(h_1 / B) - Fr_1^2}{Fr_1^2 (D / B)}]\Delta h_{1-3} \\ C_D' = f(Fr, M, B / h) \end{cases} \tag{7}$$

In Equation (7), D / B represents the water-blocking ratio of the equivalent rectangular cross-section of the bridge pier, h_1 / B is the reciprocal of the width-to-depth ratio of the equivalent rectangular cross-section, Fr denotes the incoming flow velocity, and M represents the water-blocking ratio. Thus, it can be concluded that the average drag coefficient around the pier is determined by parameters such as the incoming flow, width-to-depth ratio, and water-blocking ratio. From the perspective of energy conservation, Equation (8) is established.

$$h_b + \frac{p_b}{\rho g} + \frac{\alpha_b V_b^2}{2g} = h_g + \frac{p_b}{\rho g} + \frac{\alpha_g V_g^2}{2g} + h_{b-g} \tag{8}$$

In Equation (8), h_{b-g} represents the total head loss of the flow through cross-section $b-g$ .Since the flow in the flume is nearly uniform, Equation (8) is rewritten to obtain Equation (9).

$$\begin{cases} \alpha_b V_b = \alpha_g V_g \quad p_b = p_g \\ h_{b-g} = h_b - h_g \\ h_{b-g} = h_{w\_b-g} + h_{L\_b-g} \\ h_b - h_g = h_{w\_b-g} + h_{L\_b-g} \end{cases} \tag{9}$$

In Equation (9), h_{w_b-g} represents the local head loss, and h_{L_b-g} represents the frictional head loss along the flow path. At the y1 measurement axis, the relative backwater height at position b in front of the pier is Δh_b, and the relative backwater height at position g behind the pier is Δh_g. The expression for the lateral water-blocking effect of the pier is then derived, as shown in Equation (10).

$$\begin{cases} \Delta h_b - \Delta h_g = h_{w\_b-g} \\ h_{w\_b-g} = \xi'_{pier} \frac{V^2}{2g} \\ \Delta h_b - \Delta h_g = \xi'_{pier} \frac{V^2}{2g} \end{cases} \tag{10}$$

In Equation (10), ξ'_{pier} represents the water-blocking coefficient on the y1 measurement axis, and V_1 represents the incoming flow velocity. After dimensionless normalization of the pier's water-blocking effect, the global water-blocking effect equation is derived, as shown in Equation (11).

$$h^*(y^*) = Ae^{(\frac{y*}{B})^2} \tag{11}$$

In Equation (11), h^* represents the dimensionless head loss, and y^* represents the dimensionless position coordinate. The exact coordinate value at a specific position is substituted into Equation (11), Through calculation, the fitted values for the coefficients A and B are 0.94 and 0.73, respectively.

3.2 Validation of the Derivation of the Global Water-Blocking Effect Coefficient of Bridge Piers

Based on the experiments on the water-blocking effects with and without the pier, the observations and recordings of the water surface profile before and after the placement of the pier are shown in Figure 4.

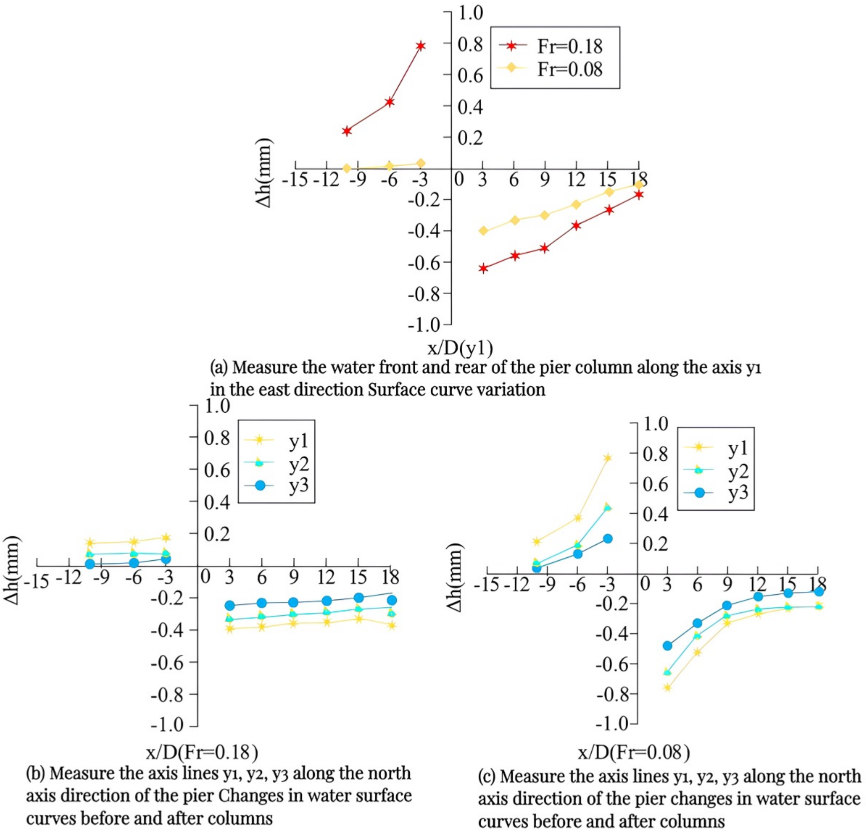

(a) Measure the water front and rear of the pier column along the axis y1 in the east direction Surface curve variation

(b) Measure the axis lines y1, y2, y3 along the north axis direction of the pier Changes in water surface curves before and after columns

(c) Measure the axis lines y1, y2, y3 along the north axis direction of the pier changes in water surface curves before and after columns

Fig. 4. Observation and recording of the water surface profile

As shown in Figure 4(a), when the flow regime parameter Fr is 0.08, the overall relative water level change is gradual, and the relative water level change is almost zero at 10D in front of the pier and 18D behind the pier, with water levels nearly matching those without the pier. When Fr is 0.18, the relative water level change is significant, indicating that the larger the Fr value, the greater the relative water level change and the more pronounced the water-blocking effect. As shown in Figures 4(b) and 4(c), the relative backwater elevation change along the measurement axes y1, y2, and y3 follows a pattern where a larger Fr value leads to a greater relative water level change, and the farther from the pier, the more gradual the water level change. To validate the effectiveness of the global water-blocking effect coefficient, experiments were conducted from both the force and energy conservation perspectives to derive the global water-blocking effect coefficient of the pier. The water-blocking effect curves under various conditions are shown in Figure 5.

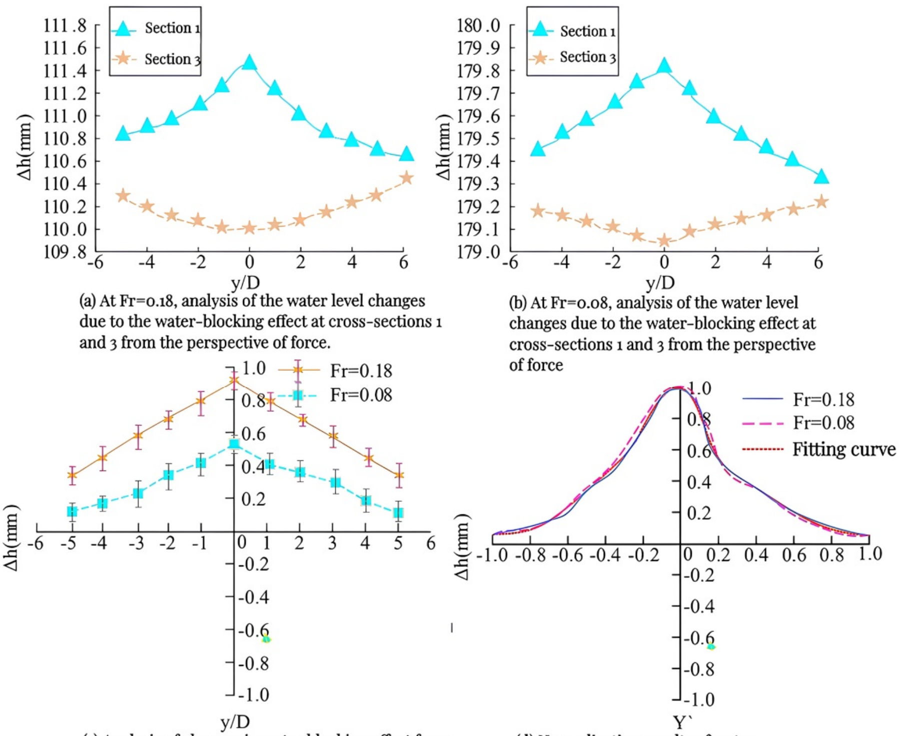

(a) At Fr=0.18, analysis of the water level changes due to the water-blocking effect at cross-sections 1 and 3 from the perspective of force.

(b) At Fr=0.08, analysis of the water level changes due to the water-blocking effect at cross-sections 1 and 3 from the perspective of force

(c) Analysis of changes in water blocking effect from the perspective of energy conservation

(d) Normalization results of water blocking effect

Fig. 5. Validation of the derivation of the global water-blocking effect coefficient of bridge piers

As shown in Figures 5(a) and 5(b), the water-blocking effect results of the pier at force angles Fr=0.18 and Fr=0.08 are 0.74 and 0.71, respectively, which are consistent with previous empirical results. It can also be observed from the figures that the water-blocking coefficients in both conditions follow a normal distribution. As shown in Figure 5(c), the water-blocking coefficient distribution along the measurement axes y1, y2, and y3 in the first condition are 0.37, 0.28, and 0.16, respectively, and in the second condition, they are 0.31, 0.22, and 0.07, respectively. Figure 5(d) shows the normalized fitting curves for the water-blocking effect distribution of the pier at two angles. From Figure 5(d), the average water-blocking effect coefficients for the two conditions are 0.17 and 0.15, respectively.

3.3 Numerical Simulation Results Analysis of the Water-Blocking Effect of Bridge Piers

To effectively perform the numerical simulation of the water-blocking effect of bridge piers and further analyze the distribution pattern of the blocking effect, the study sets the angles between the single cylindrical inclined pier and the river channel to 0°, 15°, 30°, 45°, 50°, and 60°. Numerical simulation experiments were conducted under four conditions: Fr=0.18, Fr=0.5, Fr=0.7, Fr=0.9. The results are shown in Figure 6.

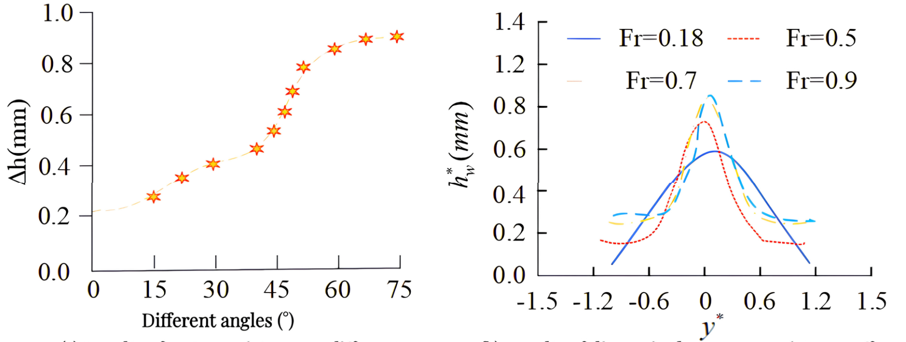

(a) Results of water resistance at different oblique angles of a single bridge pier

(b) Results of dimensionless water resistance effect under different inflow conditions

Fig. 6. Results of different conditions for the single cylindrical inclined pier

Figure 6(a) shows the water-blocking results for different skew angles of the single pier. From Figure 6(a), it can be seen that as the skew angle increases, the backwater level also gradually increases. The most dramatic change in backwater level occurs when the skew angle increases from 45° to 60°, reaching 0.41 mm. Figure 6(b) shows the dimensionless results of the numerical simulation under four different conditions. From Figure 6(b), it can be seen that with a fixed skew angle, the backwater level increases as the Fr value increases. The farther from the pier, the more gradual the backwater level change, and the results follow a normal distribution. Finally, by fitting the relationship between the Fr value and the dimensionless parameters A and B, the modified global dimensionless formula for the water-blocking effect is obtained, as shown in Equation (12).

$$h_w^*(y^*) = [0.182e^{-Fr/0.369} + 0.76]e^{-[y^*/(0.001e^{Fr/0.126}+7.714)]^2} \tag{12}$$

In Equation (12), h_w^* represents the dimensionless head loss, and y^* represents the dimensionless position coordinate. The water-blocking effect at different positions on the same cross-section is only related to the upstream flow Fr value, and all follow a normal distribution. The above results indicate that the water-blocking effect of the cylindrical inclined bridge pier increases with the flow rate and the skew angle of the river. The global dimensionless formula for the water-blocking effect proves to be practical.

3.4 Study on the Influence of Various Factors on the Backwater Magnitude Around Bridge Pier Groups

To validate the influencing factors of the water-blocking effect of bridge pier groups, the study arranged piers at dimensionless positions a, d, e, and h along the y1 measurement axis, at positions b, f, and g along the y2 measurement axis, and at positions c and g along the y3 measurement axis, and conducted hydraulic simulation experiments. The experiment is divided into two parts. The first part involves analyzing the influencing factors of the bridge pier under four hydraulic conditions, including different flow rates, depths, and upstream inflow velocities. The specific experimental conditions for this part are shown in Table 1.

Table 1. Water-blocking effect conditions for bridge pier groups under different working conditions

Test conditions	Water blocking ratio (%)	Energy coefficient	Fr	Re	Water Blocking Coefficient 1	Water Blocking Coefficient 2	Water Blocking Coefficient 3
1	5.8	0.0003	0.03	3400	0.08	0.02	0.12
2	5.8	0.0015	0.07	8900	0.09	0.04	0.18
3	5.7	0.0041	0.08	13900	0.15	0.06	0.49
4	5.7	0.0048	0.14	17900	0.29	0.14	0.71

The second part of the experiment involves selecting the water-blocking effect results for bridge piers with four different spans and analyzing the effect at different skew angles of the river. The results of the two experiments are shown in Figure 7.

From Figure 7(a), it can be seen that the water-blocking effect of the bridge piers increases with the flow rate, water depth, and upstream flow velocity, and the closer to the pier, the more significant the water-blocking effect. From Figure 7(b), it can be observed that the smaller the skew angle of the bridge pier, the more gradual the change in the backwater position; the larger the skew angle, the greater the change in the backwater position. At a skew angle of 40°, the difference in water-blocking effects for various skew angles is minimal, which can be attributed to the overlapping effect caused by the large number of piers. The results of the bridge pier experiments under different flow rates, depths, upstream flow velocities, and skew angles indicate that the water-blocking effect of the pier group increases as the flow velocity, water depth, flow rate, and skew angle increase. In summary, the derived global water-blocking formula can effectively calculate the global water-blocking coefficient of bridge piers, and the water-blocking effect of cylindrical inclined bridge piers is positively correlated with flow velocity, river depth, flow rate, and skew angle.

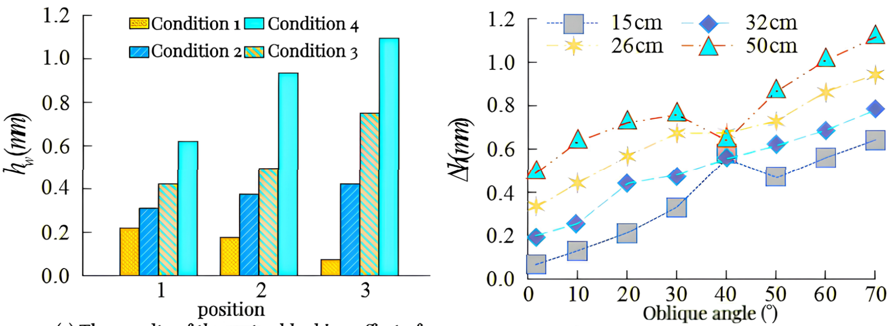

(a) The results of the water blocking effect of bridge pier groups under different conditions

(b) Results of water blocking effect of bridge piers with different oblique angles

Fig. 7. Water-blocking effect results of bridge piers with four different spans and different skew angles of the river

4 Conclusion

This study systematically analyzes the water blocking effect of circular inclined bridge piers under different flow conditions. Using CFD numerical simulation, it reveals the influence of flow velocity, flow depth, flow rate, and skew angle on the water blocking effect, providing theoretical support and data references for related engineering projects. Additionally, the study highlights the challenges and future directions of applying theoretical methods to real and complex hydraulic environments.

(1) With the increasing demand for water-related infrastructure, circular inclined bridge piers have been widely applied in practical engineering. However, their water blocking effect still requires further study.

(2) Through hydraulic model experiments, the study derived and validated the global water blocking effect coefficient and formula, identifying the key factors influencing the water blocking effect of single and multiple circular inclined bridge piers.

(3) Numerical simulations show that the water blocking effect of circular inclined bridge piers significantly increases with the rise in flow velocity, flow depth, flow rate, and pier skew angle.

(4) Experimental results indicate that the larger the flow parameters, the more pronounced the relative change in water level, leading to an enhanced water blocking effect.

(5) The validity of the proposed computational and simulation methods was verified through model tests and CFD simulation experiments, demonstrating their effectiveness in simulating the water blocking effect of inclined bridge piers.

(6) The data in this study were obtained from experimental environments, while real hydraulic environments are more complex. Future research should focus on applying theoretical methods in complex real-world environments.

References

1. Liu, L., & Yang, Y. (2021). Discussion on the impact of bridge-related water construction on rivers and mitigation measures. Three Gorges Environment and Ecology, 43(4), 59–62.
2. Sun, H., Chen, Y., Cai, F., et al. (2021). Experimental study on the hydraulic model of the water conveyance and power generation system of Baihetan Hydropower Station. Water Power Energy Science, 39(2), 89–90.
3. Lu, Y., Lu, T., Wang, Z., et al. (2012). Application of numerical simulation technology in teaching building mechanics. Higher Architectural Education, 21(2), 137–139.
4. Huang, J., Tao, T., Sun, X., et al. (2022). Influence of pier blockage ratio on the flow velocity distribution in curved rivers. Science Technology and Engineering, 22(22), 9781–9789.
5. Deng, S. (2007). Characteristics and calculation of flow resistance around pile columns. China Harbour Construction, (1), 4–6.
6. Zhang, T., Huang, W., & Li, H. (2018). Calculation and analysis of water blocking ratio for river-crossing bridges based on pier and pile resistance. Guangdong Water Resources and Hydropower, (2), 15–18.
7. Wei, S., Li, A., & Tao, B. (2022). Analysis of the impact of circular-ended pier arrangement on backwater in front of piers in rivers. Water Resources Planning and Design, (2), 72–75, 106.
8. Gao, P., Mou, X., Wang, Q., & Mei, X. (2020). Protective study of numerical simulation on circular-ended piers. Journal of Inner Mongolia Agricultural University (Natural Science Edition), 41(2), 52–55.
9. Zhao, Z., Zhou, L., Bai, L., et al. (2024). Recent advances and perspectives of CFD–DEM simulation in fluidized bed. Archives of Computational Methods in Engineering, 31(2), 871–918.
10. Yang, C., Li, Q., Hu, X., et al. (2023). Study on the effect of stagger angles between adjacent blades on waterwheel performance based on the VOF model. China Rural Water and Hydropower, 191–195.
11. Chen, J., Xi, X., Yin, H., et al. (2022). Simulation analysis of the effect of pneumatic explosion soil loosening based on EDEM-Fluent coupling. Journal of Northeast Agricultural University, 53(3), 70–79.
12. Yang, Y., Li, D., Ma, Y., et al. (2021). Fine numerical simulation of hydrodynamic characteristics in compound channels under the effect of floodplain vegetation based on Fluent simulation software. Journal of Dalian Ocean University, 36(2), 317–324.
13. Yan, W., Sun, Z., & Zhou, J. (2023). Numerical study of cascade flow using the PAFV turbulence model. Science Technology and Engineering, 23(7), 3075–3083.

14. Zeng, C., Zhang, R., Liu, M., et al. (2023). Study on the influence of different turbulence models on lead-bismuth solidification simulation. Nuclear Power Engineering, 44(1), 40–45.
15. Saiyad, A., Fulpagare, Y., & Bhargav, A. (2022). Comparison of detached eddy simulation and standard k–ε RANS model for rack-level airflow analysis inside a data center. Building Simulation, 15(9), 1595–1610.
16. Gu, C., & Dai, L. (2022). Fast numerical calculation method of the mass-conserving lubrication model. Lubrication Engineering, 47(1), 147–152.
17. Zhang, Z., Ye, S., Yue, J., et al. (2021). Multiple correction methods for Reynolds-averaged turbulence models based on combined neural networks. Chinese Journal of Theoretical and Applied Mechanics, 53(6), 1532–1542.
18. Ma, J., Jie, H., Bai, M., et al. (2023). Study on the normal restitution coefficient model based on dimensional analysis. Chinese Journal of Theoretical and Applied Mechanics, 55(4), 982–990.
19. Liu, L., Wang, X., Duan, Q., et al. (2022). Determination and countermeasures of external water pressure on lining of hydraulic tunnels in high-pressure water-rich formations. Chinese Journal of Geotechnical Engineering, 44(8), 1549–1557.